

## The Mobile Luminescence End-Station, MoLES: a new public facility at Daresbury Synchrotron

Frances Quinn,<sup>a</sup> Nigel Poolton,<sup>a\*</sup> Andrew Malins,<sup>a</sup> Emmanuel Pantos,<sup>a</sup> Claus Andersen,<sup>b</sup> Phil Denby,<sup>a,b</sup> Vin Dhanak<sup>a</sup> and George Miller<sup>a</sup>

<sup>a</sup>Synchrotron Radiation Department, Daresbury Laboratory, Daresbury, Warrington WA4 4AD, UK, and <sup>b</sup>Radiation Research Department, Risø National Laboratory, DK-4000 Roskilde, Denmark. E-mail: n.r.j.poolton@dl.ac.uk

A new mobile end-station is described for use on multiple beamlines at the Daresbury synchrotron radiation source (overall excitation range 5 eV to 70 keV) that allows for the detection and dispersion of photoluminescence from solid-state samples in the emission range 190–1000 nm (1.2–6.5 eV). The system is fully self-contained and includes sample-cooling facilities for the temperature range 8–330 K using a closed-cycle refrigerator, thus eliminating the need for liquid cryogenics. The system also includes solid-state laser sources for use with a variety of pump–probe-type experiments, and an Ar<sup>+</sup> surface-cleaning facility. In order to demonstrate the various capabilities of the system, the results of a variety of experiments are summarized, carried out over the excitation range 5–5000 eV on beamlines 3.2, MPW6.1 and 4.2. These include the optical detection of XAS of *L*-edge structure in natural minerals and archaeological ceramics, band-gap determinations of wide-band-gap silicates, and pump–probe studies of quartz.

**Keywords:** luminescence; lasers; pump–probe; OD-XAS; quartz; feldspar.

### 1. Introduction

Studying the luminescence excitation and emission processes in solid-state matter can provide valuable insights into the energy transfer processes that occur in the materials, and details of both the host lattices and defects contained within them. Synchrotron radiation is an ideal stimulation source for such studies, since its tunability potential means that a wide range of excitation/relaxation pathways can be explored. Furthermore, the high intensity allows dilute or small sample quantities to be probed (e.g. Elango *et al.*, 1983; Soderholm *et al.*, 1998; Kink *et al.*, 1998; Belsky & Krupa, 1999; Mikhailin, 2000).

Many synchrotron facilities worldwide have dedicated beamlines and end-stations for the study of luminescence phenomena [e.g. beamline 1 (SUPERLUM1) at Hasylab, Germany; beamline U9B at the National Synchrotron Light Source, USA]. At the Daresbury SRS, beamline 13.1 is used for confocal fluorescence microscopy imaging and fluorescence decay measurements (Martin-Fernandez *et al.*, 1998; O'Donnell *et al.*, 1999). However, to utilize the wider range of excitation energies available on other relevant beamlines of the SRS (e.g. in the range 4 eV–70 keV), luminescence excitation and emission systems have, until now, been assembled on an *ad hoc* basis to meet the specific purposes of individual research teams for each experiment.

As part of Daresbury's strategy of improving instrumentation function and flexibility, and making synchrotron radiation facilities available to a wider user community, EPSRC has funded the

**Table 1**

Directly compatible beamlines for MoLES at the SRS, Daresbury.

Beamline	Energy (eV)	Beamline	Energy (keV)
3.1	4–30	4.2	0.64–10
3.2	5–35	7.2	8.3 or 9.7
3.3	10–120	2.1	8
5D.1	20–200	16.1	8.8
MPW6.1	30–450	MPW6.2	6–18
4.1	15–200	16.2	9.1 or 23.8
5U.1	60–1000	9.8	9–40
1.1	225–1200	16.3	5–70

construction and development of a public utility Mobile Luminescence End-Station (MoLES), for use on multiple beamlines at the SRS. This article describes the experimental capabilities of the new MoLES system, together with examples of the wide range of experiments that have been carried out during the commissioning phase. Table 1 presents a summary of the different beamlines for which MoLES is directly compatible. The construction of MoLES complements a range of other peripatetic spectrometers and end-stations currently available for use within the SRS facility. These are mainly electron photoemission spectrometers, and (X-ray) fluorescence-yield detectors.

### 2. Equipment

#### 2.1. Sample chamber and light-collection optics

The sample chamber consists of a miniature stainless steel Kimball Physics UHV 'spherical square' chamber, with an inner diameter of 13 cm. As mounted, up to eight ports are available for optical access, although at present only five are utilized as such. Fig. 1 shows a representative arrangement of the ports as currently used. The chamber has a dedicated turbo pumping system, with non-bake base pressures of typically  $10^{-8}$  torr at room temperature, or  $<10^{-10}$  torr at 10 K.

For excitation in the vacuum-ultraviolet/soft X-ray regions (6.5 eV to  $\sim 3$  keV) the pumped UHV chamber is connected directly to the beamlines, with the option of additional VUV contamination/order-

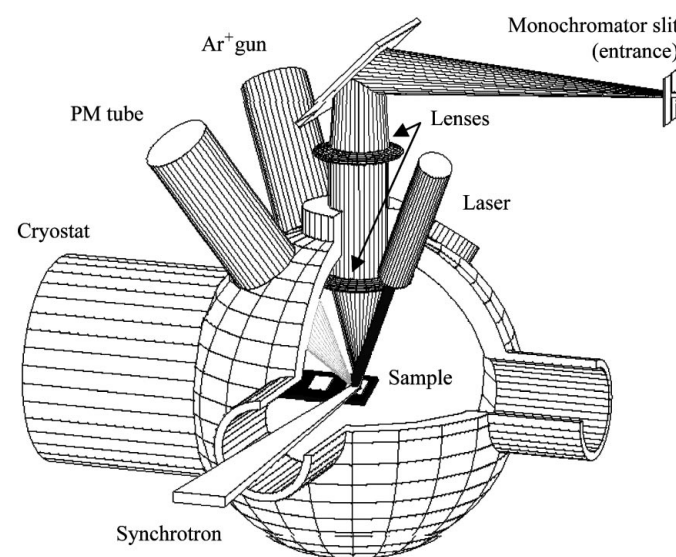


**Figure 1**

Schematic cut-away section of the MoLES luminescence sample chamber (inside diameter 13 cm), with relative coordinations of the optical access and sample ports. For XUV synchrotron stations, no entrance window is used (as shown here). For clarity, only the entrance slit of the spectrograph/monochromator is shown.

sorting filters. For harder X-ray irradiation an aluminized mylar vacuum window can be employed, replaceable with a simple quartz window for very low energy excitation (0.5–6.5 eV).

The system has been designed to detect weakly luminescent systems. To maximize light collection, an  $f1.4$  collimating lens is located *inside* the vacuum chamber directly above the sample (see Fig. 1). Luminescence then passes through the main central window of the chamber, re-focusing at the spectrograph slit so as to accept the ‘letter box’ footprint of the synchrotron source. Two orthogonal alignment lasers are incorporated so as to ensure accurate positioning of the sample, synchrotron beam, light-collection optics and probe lasers (see §2.5).

Of the four remaining ports surrounding the principal luminescence exit window, one is used for observation and a second carries the 0.1–3 keV Ar<sup>+</sup> surface-cleaning unit. The final two are used, respectively, for laser excitation and broad-band luminescence detection, where standard optical filters can be employed.

All the windows and lenses use low-fluorescence UV-grade fused silica (*e.g.* Spurasil-1 or equivalent), with typical transmissions better than 85% from 0.6 to 6.7 eV (185 to 2000 nm).

## 2.2. Spectrograph

Spectral dispersion is achieved using a compact imaging spectrograph (Triax-190, from Jobin-Yvon). This is a high-efficiency 19 cm focal-length instrument with  $f3.9$  optics, the choice of three gratings,

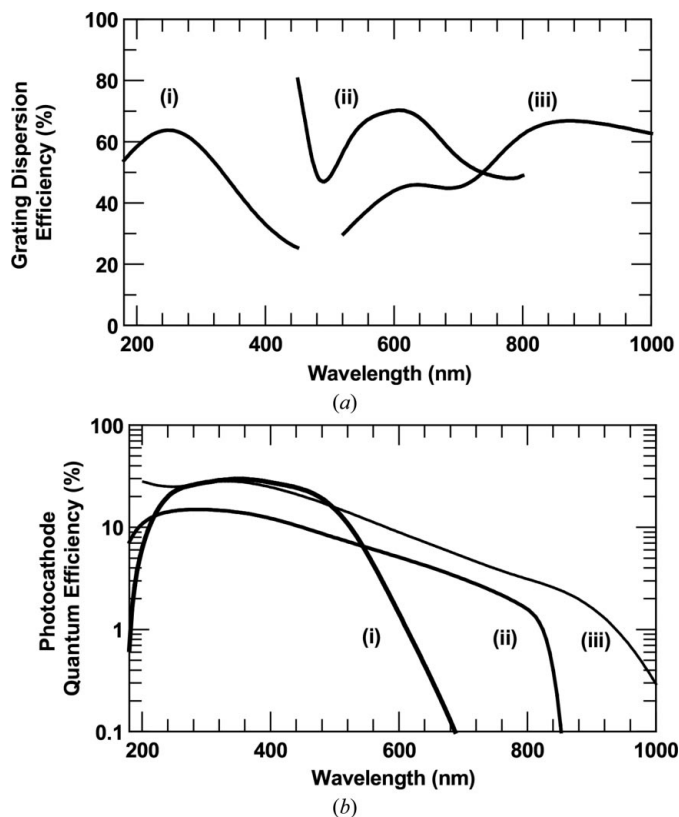


**Figure 2** (a) Dispersion efficiencies of the three gratings (1200 lines mm<sup>-1</sup>) presently used in MoLES, blazed at (i) 250, (ii) 630 and (iii) 900 nm. The gratings are commercially available from [www.jyhoriba.com](http://www.jyhoriba.com). (b) Quantum efficiencies of the photomultiplier photocathodes, as used in MoLES for (i) bialkali, (ii) GaAs and (iii) GaInAs:Ce photocathodes. For full information, see [www.electrontubes.com](http://www.electrontubes.com) and [www.hamamatsu.com](http://www.hamamatsu.com).

and option of two orthogonal exit apertures. At present, both exits have slits installed, for use with photon-counting detectors.

The diffraction gratings presently used disperse in the range 1.2–6.5 eV (190–1000 nm), being blazed at 250, 630 and 900 nm, respectively; their unpolarized diffraction efficiencies are shown in Fig. 2(a). At 1200 lines mm<sup>-1</sup> the gratings provide dispersions of 3.5 nm mm<sup>-1</sup> at the slit plane, so the resolution of the system is variable from 7 nm (best throughput) to 0.3 nm (best resolution).

## 2.3. Light detection

Three photomultipliers are available for use with the system, covering the spectral range 190–1020 nm (see Fig. 2b); all have low dark counts for use in photon-counting mode. The bialkali tube (Electron Tubes, 9111WB) is in the form of a miniature self-contained photon-counting unit (TTL output), and is typically used for high-sensitivity broad-band luminescence detection. Count rates of up to 10<sup>8</sup> counts s<sup>-1</sup> are possible with pulse-pair resolution of 10 ns; the dark count rate is 20 counts s<sup>-1</sup>.

For detection over extended photon ranges, GaAs-based photocathode tubes are used; these are also more amenable for time-resolved studies. The spectral responses of the GaAs and GaInAs:Ce photocathode (Hamamatsu R2949 and R2658P, respectively) are also shown in Fig. 2(b). At room temperature the GaAs tube (typical gain 10<sup>7</sup>) has dark counts of around 300 counts s<sup>-1</sup>. Cooling is also an option, since it uses the same thermoelectric housing as the GaInAs tube (typical gain 1.6 × 10<sup>5</sup>), whose dark counts reduce from around 10<sup>4</sup> to 50 when cooling to 258 K (30 min cool-down).

## 2.4. Sample cooling: the cryostat

MoLES incorporates a compact low-temperature UHV-compatible cryostat. This is a two-stage Gifford McMahon closed-cycle refrigerator (modified Advanced Research Systems CSW-202B) providing 0.4 W of cooling power at 8 K (2.5 W at 20 K) and a full temperature range of 7–330 K. PID temperature control is provided via a Lakeshore (model 331S) control unit, with 0–50 W heating power available. The advantages of closed-cycle refrigeration are that no liquid cryogenics are necessary, and cooling is simply a ‘push button’ operation. Typical cool-down times to 10 K are 90 min; see Fig. 3.

The cryostat is mounted on a motorized runway, allowing the position of the cold sample finger to be moved by up to 30 mm relative to the synchrotron beam position.

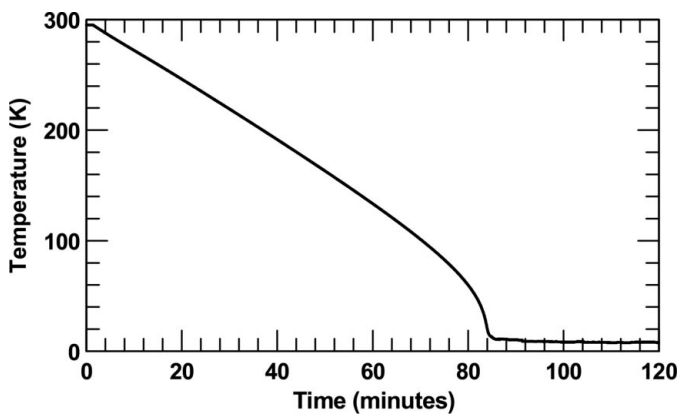


**Figure 3** Cool-down characteristics for the closed-cycle refrigerator incorporated in MoLES. The base temperature achievable during synchrotron stimulation of samples is typically 10 K. For full refrigerator details, see [www.arscryo.com](http://www.arscryo.com).

### 2.5. Secondary excitation sources: lasers

Two solid-state lasers are available for use with MoLES, acting as either primary excitation sources (*e.g.* for off-line work) or as secondary ‘probe’ sources with synchrotron-pump studies. These are, respectively, a 10 mW, 532 nm frequency-doubled YAG and a 5 mW, 404 nm Nichia semiconductor laser diode.† Both sources incorporate optics for variable focusing at the sample, and can access any of the optical ports as shown in Fig. 1. The use of other laser/optical stimulation sources can easily be incorporated using fibre-optic couplings.

### 3. Examples of luminescence-based measurements using MoLES

During commissioning, MoLES has been applied to a variety of multi-disciplinary investigations, from the analysis of archaeological ceramics to the investigation of luminescence processes in quantum dots. In the following sections we highlight recent results provided by MoLES that demonstrate the various capabilities of the system. These were carried out on a number of beamlines at the SRS, Daresbury, using exciting photon energies in the range 5 eV to 5 keV (beamlines 3.2: 5–40 eV; MPW6.1: 30–450 eV; and 4.2: 2–5 keV).

#### 3.1. Optical band-gap determination in wide-band silicates, 10–300 K

The optical band-gaps of semiconductors and insulators play a major role in determining the electronic and optical properties of the materials. They can be measured using a variety of methods, including (most obviously) optical absorption (OA) and reflection electron energy-loss spectroscopy (REELS) [*e.g.* for SiO<sub>2</sub>, see Bosio & Czaja (1993) and Bart *et al.* (1994), respectively]. However, these methods require considerable care in sample/surface preparation prior to measurement, and this is not always expedient. Conversely, luminescence excitation spectroscopy offers a simple and effective method of measurement, not only of the high-mobility band edge but also for probing the Urbach tail and determining threshold energies for exciton absorption. Previous examples can be found for semiconductors InAlAs (Roura *et al.*, 1997), CdS (Ullrich *et al.*, 1999), EuSe (Akimoto *et al.*, 1996) and wide-gap insulators SiO<sub>2</sub> (Itoh *et al.*, 1989), PbCl<sub>2</sub> and PbBr<sub>2</sub> (Kink *et al.*, 1998).

As the near-edge band structure for crystalline quartz is well known, we have demonstrated that MoLES is ideally suited to band-edge studies by measuring the luminescence excitation spectra for natural hydrothermal quartz (Bourg d’Oisans, France) on SRS station 3.2, as shown in Fig. 4(a) (Malins *et al.*, 2003). The sample surface is simply prepared by HF etching of a *z*-cut single-crystal slice. The main temperature variation of the spectra in the range 8–300 K derives from well known thermal quenching of the recombination part of the luminescence cycle (Alonso *et al.*, 1983). For excitation below the band-gap energy, a range of deep-lying defect centres are directly probed, giving rich structure in the range 5–8 eV. The indirect band-gap is immediately apparent from Fig. 4(a) at low temperatures by the rapid cut-off in luminescence excitation efficiency between 8.5 and 9 eV. By differentiating this part of the spectrum, the gap is determined to be 8.7 eV, which directly corresponds with that measured by Bart *et al.* (1994) using REELS. The above band-gap excitation spectra up to 30 eV are also rich in structure. For example, a broad peak is observed at 21 eV, probably associated with surface plasmons. Furthermore, the presence of the direct band gap is also apparent in Fig. 4(a) from the trench at 10.5 eV (onset 10.2 eV),

† The 404 nm laser is available on loan from Professor D. Eastham. The 532 nm laser is a *bona fide* component of MoLES.

almost certainly deriving from the well known exciton absorption at this energy (Bart *et al.*, 1994).

MoLES has been used to examine systems where the band edges have never been examined before, such as the aluminosilicate feldspars (Malins *et al.*, 2003). Fig. 4(b) shows a variable-temperature luminescence excitation plot for the particular example of NaAlSi<sub>3</sub>O<sub>8</sub> feldspar. Many features are directly comparable with that of quartz, including the thermal quenching of the emission and the presence of defect states at lower energies. The band-edge is very distinct and has been determined to be 7.7 eV at 8 K; this decreases slightly as the temperature is raised, to 7.5 eV at 300 K. Above band-gap excitation is largely devoid of the features observed in quartz, partly suggesting a direct nature of the band gap in this material.

#### 3.2. Optically detected XAS (OD-XAS) in minerals

If luminescence excitation spectroscopy can be used to determine the optical band-gap energies of insulator crystals (§3.1), it can

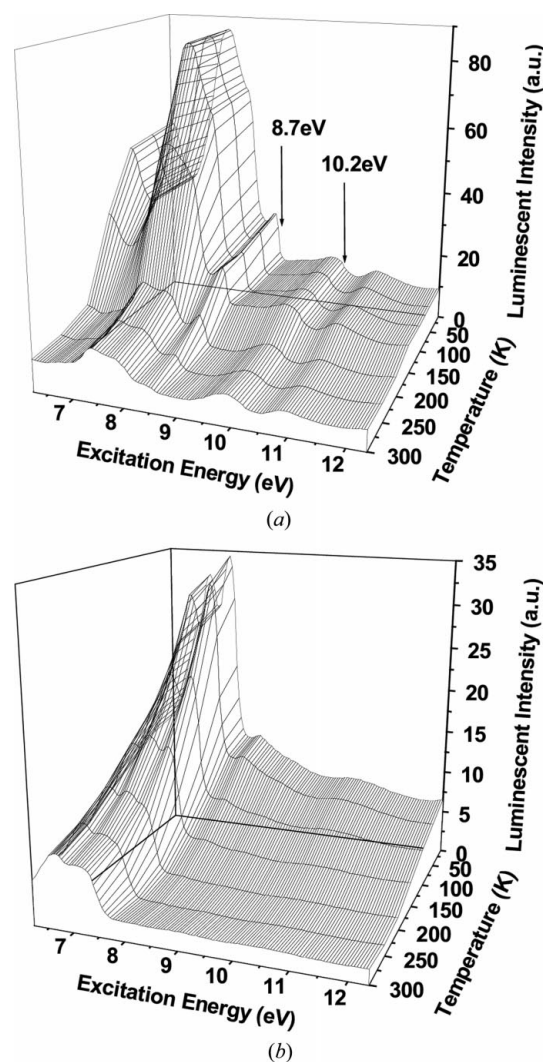


**Figure 4** Temperature-dependent luminescence excitation characteristics of natural crystalline samples of (a) quartz (SiO<sub>2</sub>) and (b) sodium feldspar (NaAlSi<sub>3</sub>O<sub>8</sub>) across the band edges, using MoLES. In both cases, broad-band detection is used, centred at  $3.6 \pm 0.4$  eV. The band edges are clearly defined by the rapid cut-off in the luminescence emission when increasing the stimulation energy; these are measured at between 7.5 eV (feldspar, 300 K) and 8.7 eV (quartz indirect gap). Luminescence stimulated using sub-band-gap excitation derives from deep-lying defect centres.

equally be applied to determine the chemical composition and local structure of the constituent atoms, when detecting visible/UV luminescence during excitation across the atomic *L*, *K* etc. edges. This is possible because the energy transfer mechanisms that occur in the lattice (that finally result in the emission at point defects in the sample) change near the atomic absorption edges (e.g. Soderholm *et al.*, 1998). This optical detection of the X-ray absorption spectra (OD-XAS) has successfully been used in studying a range of materials, such as bulk CaF<sub>2</sub> (Ca *K*, *L* edges; Bianconi *et al.*, 1978; Naftel *et al.*, 2001), oxides such as Al<sub>2</sub>O<sub>3</sub>, MgO, SiO<sub>2</sub> (Al, Mg, Si *L* edges; Elango *et al.*, 1983), and porous silicon (Gardelis *et al.*, 1996). Its sensitivity has been demonstrated by using the method to study trace impurities in Gd<sub>2</sub>O<sub>3</sub>-based materials (Soderholm *et al.*, 1998). The advantages of OD-XAS/EXAFS over conventional methods of detection are its sensitivity, selectivity (only luminescent phases are monitored) and the added information derived concerning energy transfer mechanisms in the lattice.

MoLES has been used to examine the XAS of feldspars minerals (Poolton *et al.*, 2003); these materials form naturally as a tertiary system with end-members CaAl<sub>2</sub>Si<sub>2</sub>O<sub>8</sub>, NaAlSi<sub>3</sub>O<sub>8</sub> and KAlSi<sub>3</sub>O<sub>8</sub>, where the *K* edge of oxygen and *L* edges of Si and Al are clearly identified *via* OD-XAS. However, it is the *L*-edge structure of Ca, K and Na that is of particular interest, since the presence of the peaks can be used as spectroscopic thumbprints, identifying the mineral composition of the luminescent mineral phase (of use, for example, in geological dating applications). Hitherto this has been unachievable. In the case of Ca and K, the detailed *L*-edge structures are directly understandable within the framework of crystal field theories developed for *d*<sup>0</sup> ions by deGroot *et al.* (1990). Fig. 5 shows an example of the OD-XAS signatures of K and Ca in representative end-member feldspars KAlSi<sub>3</sub>O<sub>8</sub> and CaAl<sub>2</sub>Si<sub>2</sub>O<sub>8</sub>, respectively, measured using beamline MPW6.1 of the SRS. The corresponding luminescence emissions, from which the signals are derived, are shown as insets to the figure: each band gives rise to the same OD-XAS signatures.

### 3.3. OD-XAS applications to ancient and modern ceramics

MoLES is currently being employed to study both ancient and modern ceramics and glazes, since the OD-XAS can provide useful insights into the methods of production and provenance of archaeological artefacts. Boron is of particular interest, since Fleet & Liu (2001) have shown that the post *K*-edge boron structure is a strong indicator of the local environment of the atom in oxides (coordination, bond length *etc.*). There is also an outstanding question as to if, when and where it was used as a flux in slip preparation (Birch, 1873). Borax is commonly used in modern pottery production as a defloculant, but boron is not easily identified using standard analyses such as XRF or SEM/EDX because of the low energy of its *K* edge (around 190 eV).

Fig. 6(b) shows the detailed OD-XAS of boron obtained using MoLES from a typical modern glaze, together with vignettes of the other OD-XAS signatures found for the same sample in the excitation range 40–600 eV (Fig. 6c). The detailed emission spectrum from

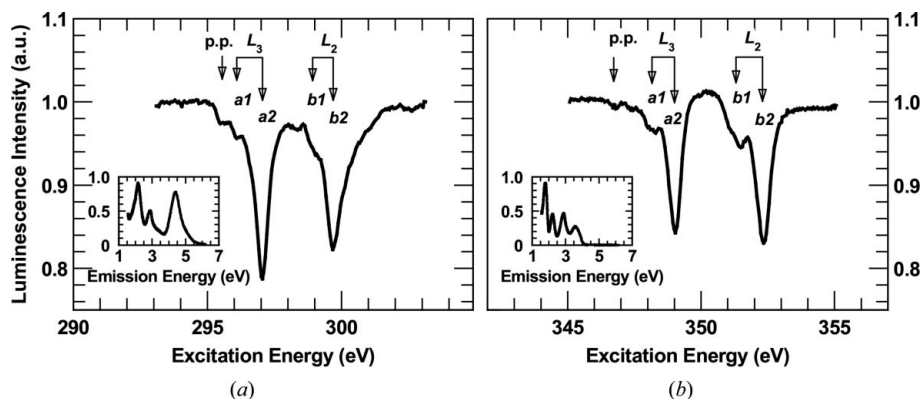


**Figure 5** Variation of the photoluminescence yield at 10 K, in (a) KAlSi<sub>3</sub>O<sub>8</sub> and (b) CaAl<sub>2</sub>Si<sub>2</sub>O<sub>8</sub>, when excitation is scanned across the fundamental *L*<sub>2,3</sub> edges of K and Ca in the materials (optically detected XAS). The detailed structure is due to crystal-field splitting of the transitions, labelled after the work of deGroot *et al.* (1990), who analysed the *L*-edge structure of *d*<sup>0</sup> ions in the potassic halides (p.p. = ‘pre-peak’). The energy-resolved spectra of the luminescence being monitored are shown in the insets.

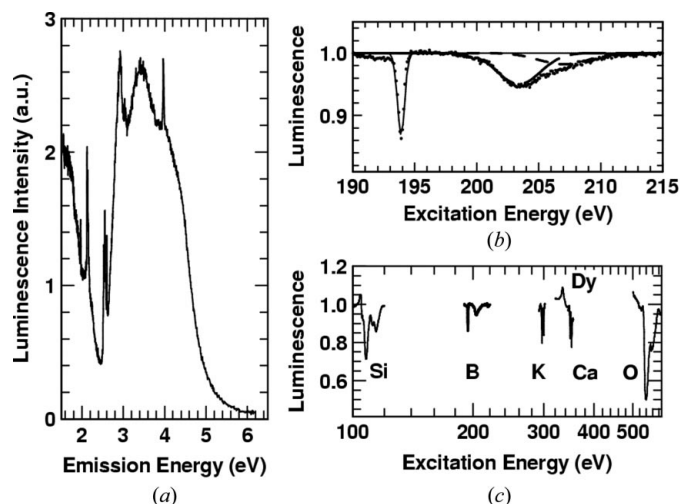


**Figure 6** (a) Luminescence emission (300 K; 140 eV excitation) of a typical modern porcelain glaze; the sharp features arise from trace quantities of Dy<sup>3+</sup>. (b) OD-XAS (10 K) observed from this emission, when stimulating over the boron *K* edges. The post-edge features depend strongly on the B–O bond lengths and coordination. (c) OD-XAS (10 K) over a wider excitation range: the *L* edges of Si, K and Ca are observed, together with the *K* edges of B and O. The Dy *N*-edge assignment is only tentative.

which the OD-XAS were derived is shown in Fig. 6(a): here the sharp features of the spectrum indicate the presence of trace quantities of rare earth impurities (Götze *et al.*, 1999), Dy<sup>3+</sup> in this case, which can again be used as further indicators of provenance.

OD-XAS has been used to analyse the Ca-containing mineral phases of the distinctive ‘black gloss’ ceramics from the Agora of ancient Athens and from Etruria, as part of an effort to understand the methods of production. The OD-XAS signals are found to be highly sensitive to the calcium concentration and composition, and the relative sign of the spectra is found to change from positive to negative as a direct consequence of variations in the Ca concentration. Very low quantities (typically <1% CaO by weight) give rise to positive-sign Ca *L*-edge excitation spectra, which become reversed at higher concentrations (e.g. >5 wt% Ca). A similar reversal is also observed for samples of low Ca concentration as the temperature is decreased from 300 K to 10 K, even though the overall luminescence

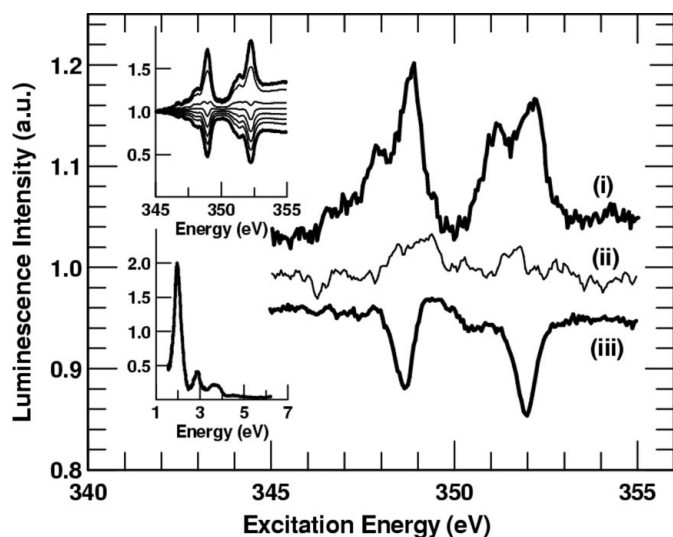


**Figure 7**  
OD-XAS (300 K) of archaeological black-gloss pottery over the Ca  $L_{2,3}$  edges, for samples with different Ca content. Curves (i) and (ii) are from the gloss, where the CaO concentrations are 0.55 and 1.20 wt%, respectively. Curve (iii) is from the ceramic body whose CaO content is 11.3 wt%. Inset top left: the simulated excitation spectra (normalized) for a range of values of the concentration parameter over an order of magnitude. Inset bottom left: emission spectrum from the ceramic body: this is dominated by the emission of  $Mn^{2+}$ .

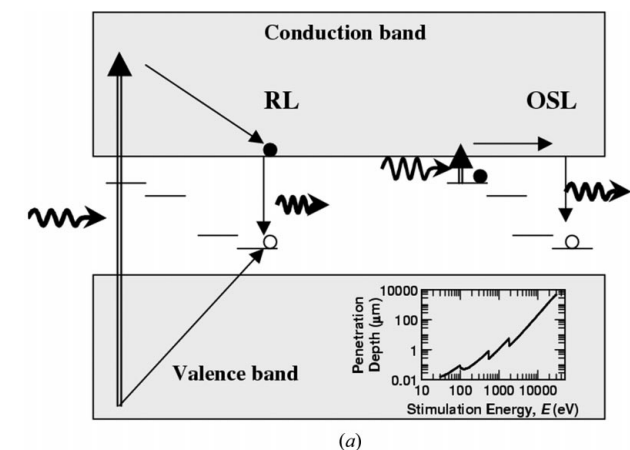
quantum yield increases. This behaviour can be modelled using the concepts of Förster-type radiationless transfer and electron-hole pair annihilation at the sample surface (Förster, 1959; Pantos *et al.*, 2003), and examples of both experimental and modelled data are given in Fig. 7. These effects are universal and are not confined to archaeological ceramics; we have seen similar behaviour in Si quantum-dot systems, and they were originally observed and modelled in benzene-doped rare-gas crystals (see Hasnain *et al.*, 1977).

### 3.4. Pump-probe luminescence

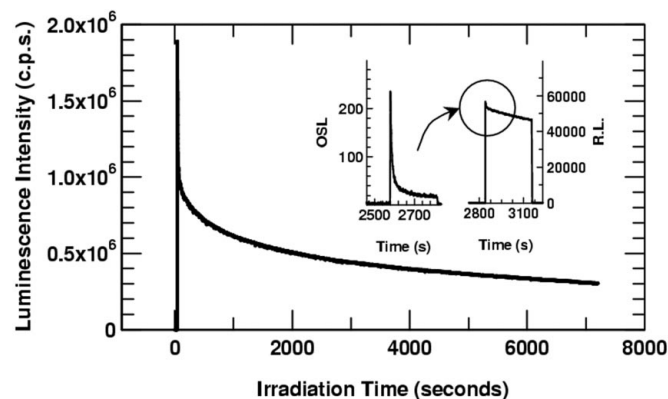
During high-energy luminescence excitation of many wide-band-gap materials, the emission intensity often evolves slowly with time, owing to charge competition and trapping at deep-lying defect states. This effect has practical implications, such as in geological dating of silicates and medical applications like *in vivo* radiation dosimetry using alumina (*e.g.* Trautmann *et al.*, 1999; Polf *et al.*, 2002).

The 10 mW, 532 nm (2.3 eV) laser attached to MoLES has been installed for the specific purpose of probing the mechanisms of charge-trapping processes in wide-gap materials under synchrotron radiation. The penetration depth of synchrotron radiation (*e.g.* in quartz) typically varies from 20 nm at 40 eV to 0.2 mm at 10 keV, so it is possible to distinguish between any surface states that may contribute to the luminescence with those present in the bulk, or to monitor variation in the recombination kinetics.

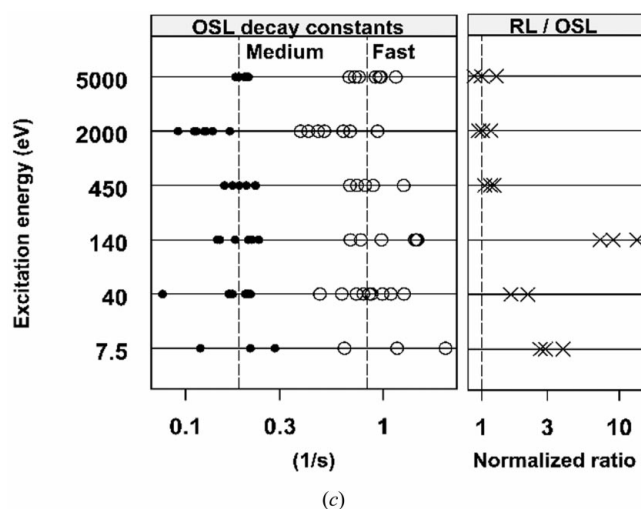
Fig. 8 summarizes typical results that have been obtained with MoLES, showing the effects of charge trapping in natural sedimen-



(a)



(b)



(c)

**Figure 8**

(a) Schematic of the mechanism of radioluminescence (RL) in wide-band-gap materials: luminescence results from the recombination of excited electrons and trapped holes. During RL, deep traps become filled with charge: the quantity of these charges can be assessed by probing with a low-energy laser, which gives rise to time-decaying anti-Stokes shifted optically stimulated luminescence, OSL. Since the penetration depth of the RL excitation photons is dependent on energy (inset: data compiled from tables provided by <http://cindy.lbl.gov>), tuning this energy allows for the probing and examination of both surface and bulk defects. (b) Dynamics of the RL signal in natural sedimentary quartz, for prolonged RL exposure. If the exposure is halted, the OSL can be used to assess the amount of trapped charge (inset left). Exposing with the laser, however, causes further redistribution of charge in the material; this gives rise to a transient in the RL if this is then continued (inset, right). (c) For the quartz sample studied, the nature of the defects is invariant with depth, as indicated by the independence of the OSL recombination kinetics, after exposure to ionizing radiation of different energies: curve fitting reveals three first-order components, the 'fast' and 'medium' being dominant; their time constants are plotted here. However, the strong variation in the relative amount of OSL and RL produced, depending on RL stimulation energy, reflects a change in either the defect distributions or in the competition for charge between the defects.

tary quartz material (Andersen *et al.*, 2003). The samples are in the form of 100–200  $\mu\text{m}$ -diameter grains, HF etched and annealed at 1073 K to remove all trapped charge from accessible defect centres. When exciting with photons of energy greater than the band gap, radioluminescence (RL) results, as the charge relaxes and recombines at (initially empty) defect levels (Fig. 8a). However, owing to competition with trapped charge (which changes during stimulation), the RL intensity evolves with time, in this case by reducing in intensity. Such effects are well known, and have been generally modelled (Trautmann *et al.*, 1999). It is the population of these competing defects that can be probed with the laser, since the low-energy stimulation causes de-trapping of the centres, resulting in optically stimulated luminescence (OSL). The re-distribution of charge induced by the laser also results in transients observed in subsequent RL (Fig. 8b, inset).

In the case of the quartz described here, the nature of the trapping centres is found to be invariant with probe depth, since the OSL recombination kinetics remain unchanged with the ionizing radiation energy (see Fig. 8c). However, the relative intensities of the RL and OSL do alter considerably, reflecting either a depth-dependent change in the populations of the luminescent and non-luminescent defects, or a significant alteration in charge-trapping competition, across the energy range.

#### 4. Conclusions and future developments

The new Mobile Luminescence End-Station (MoLES) has been shown to have a wide range of applications in both luminescence excitation and emission spectroscopy of solid-state samples. The compact nature of the system makes it ideally suited to incorporation on many SRS beamlines, and the multiple ports of the chamber have been used for the purposes of double excitation of the samples. This feature also means that the system can easily be developed to allow for a range of multiple-detection/excitation methods. Future plans are to incorporate XRF detectors, electrical conductivity capability and miniature electron analyser systems to allow for simultaneous luminescence/photoelectron/conductivity detection.

The work has been made possible by the provision of funding in the UK by EPSRC, grant number GR/R88410/01, and SRS beam time awards 39115 and 39116. Grants provided to NP and CA by Risø National Laboratory for travel between Denmark and the UK are also gratefully acknowledged.

#### References

- Akimoto, R., Kobayashi, M. & Suzuki, T. (1996). *J. Phys. Condens. Matter*, **8**, 105–110.
- Alonso, P. J., Halliburton, L. E., Kohnke, E. E. & Bossoli, R. B. (1983). *J. Appl. Phys.* **54**, 5369–5375.
- Andersen, C. E., Poolton, N. R. J., Malins, A. E. R., Pantos, E., Bøtter-Jensen, L., Murray, A. S. & Quinn, F. M. (2003). In preparation.
- Bart, F., Gautier, M., Jollet, F. & Duraud, J. P. (1994). *Surf. Sci.* **306**, 342–358.
- Belsky, A. N. & Krupa, J. C. (1999). *Displays*, **19**, 185–196.
- Bianconi, A., Jackson, D. & Monahan, K. (1978). *Phys. Rev. B*, **17**, 2021–2024.
- Birch, S. (1873). *History of Ancient Greek Pottery*, p. 174. London: John Murray.
- Bosio, C. & Czaja, W. (1993). *Europhys. Lett.* **24**, 197–201.
- deGroot, F. M. F., Fuggle, J. C., Thole, B. T. & Sawatzky, G. A. (1990). *Phys. Rev. B*, **41**, 928–937.
- Elango, M., Prүүлmann, T. & Zhurakovskii, A. P. (1983). *Phys. Status Solidi B*, **115**, 399–407.
- Fleet, M. E. & Liu, X. (2001). *Phys. Chem. Miner.* **28**, 421–427.
- Förster, T. (1959). *Discuss. Faraday Soc.* **27**, 7–17.
- Gardelis, S., Bangert, U., Hamilton, B., Pettifer, R. F., Hill, D. A., Keyse, R. & Teehan, D. (1996). *Appl. Surf. Sci.* **102**, 408–412.
- Götze, J., Habermann, D., Neuser, R. D. & Richter, D. K. (1999). *Chem. Geol.* **153**, 81–91.
- Hasnain, S. S., Hamilton, T. D. S., Munro, I. H., Pantos, E. & Steinberger, I. T. (1977). *Philos. Mag.* **35**, 1299–1316.
- Itoh, C., Tanimura, K., Itoh, N. & Itoh, M. (1989). *Phys. Rev. B*, **39**, 11183–11186.
- Kink, R., Avarmaa, T., Kisand, V., Löhmus, A., Kink, I. & Martinson, I. (1998). *J. Phys. Condens. Matter*, **10**, 693–700.
- Malins, A. E. R., Poolton, N. R. J., Quinn, F. M. & Johnsen, O. (2003). Submitted.
- Martin-Fernandez, M. L., Tobin, M. J., Clarke, D. T., Gregory, C. M. & Jones, G. R. (1998). *Rev. Sci. Instrum.* **69**, 540–543.
- Mikhailin, V. V. (2000). *Nucl. Instrum. Methods*, **A448**, 461–466.
- Naftel, S. J., Yiu, Y. M., Sham, T. K. & Yates, B. W. (2001). *J. Electron Spectrosc. Relat. Phenom.* **119**, 215–220.
- O'Donnell, K. P., Trager Cowan, C., Pereira, S., Bangura, A., Young, C., White, M. E. & Tobin, M. J. (1999). *Phys. Status Solidi B*, **216**, 157–161.
- Pantos, E., Poolton, N. R. J., Malins, A. E. R., Quinn, F. M. & Prag, A. J. N. W. (2003). In preparation.
- Polf, J. C., McKeever, S. W. S., Akselrod, M. S. & Holmstrom, S. (2002). *Radiat. Prot. Dosim.* **100**, 301–304.
- Poolton, N. R. J., Malins, A. E. R., Quinn, F. M., Pantos, E., Andersen, C. E., Bøtter-Jensen, L., Johnsen, O. & Murray, A. S. (2003). *J. Phys. D*, **36**, 1107–1114.
- Roura, P., López-de Miguel, M., Cornet, A. & Morante, J. R. (1997). *J. Appl. Phys.* **81**, 6916–6920.
- Söderholm, L., Liu, G. K., Antonio, M. R. & Lytle, F. W. (1998). *J. Chem. Phys.* **109**, 6745–6752.
- Trautmann, T., Krbetschek, M. R., Dietrich, A. & Stolz, W. (1999). *J. Lumin.* **85**, 45–58.
- Ullrich, B., Bagnall, D. M., Sakai, H. & Segawa, Y. (1999). *Solid State Commun.* **109**, 757–760.